Far-infrared spectroscopy of minibands and confined donors in GaAs/$Al_xGa_{1-x}As$ superlattices

M. Helm,* F. M. Peeters,† F. DeRosa, E. Colas, J. P. Harbison, and L. T. Florez
Bellcore, Red Bank, New Jersey 07701-7040
(Received 13 November 1990)

We present a far-infrared-absorption study of electrons in lightly doped GaAs/$Al_xGa_{1-x}As$ superlattices. A grating coupler enables us to observe transitions that require an electric-field polarization along the superlattice axis. We investigate weakly and strongly coupled superlattices, and demonstrate the difference between intersubband transitions and transitions between extended minibands. The line shape of the interminiband absorption deviates considerably from the predictions of a simple single-particle model. We discuss possible reasons in terms of fluctuations and localization. At low temperatures, the absorption spectra are dominated by donor transitions. The transition from the donor ground state to the pure $2p_z$ state, which is associated with the second subband, is observed. In a variational calculation, we compute the four-lowest donor states for a variety of superlattice parameters. Excellent agreement between experiment and theory is achieved.

I. INTRODUCTION

Confinement of electrons in quantum wells or superlattices leads to the formation of a variety of electronic states like subbands in quantum wells or minibands with a finite dispersion, if the interwell coupling is strong enough.[1] In addition, the impurity states are significantly modified by the confinement.[2] Besides interband optical spectroscopy, where both electrons and holes have to be considered, intraband spectroscopy is an effective method to study these states. The pioneering work was the intersubband absorption experiment by West and Eglash.[3] This work, like many others, was performed with heavily (modulation) doped structures in order to achieve high absorption coefficients, which is important for the application as infrared detectors.[4] On the other hand, only lightly doped structures, where collective effects are negligible, can provide accurate information about the single-particle states.

Transitions between states that arise from confinement in the growth direction can only be excited with light that has an electric-field component in this direction.[5] This requires special coupling techniques like Brewster angle[3] or waveguide[6] geometries. An alternative is the use of a grating coupler,[7] which allows normal-incidence transmission experiments.[8–13]

In this paper we report grating-coupler-induced intersubband absorption measurements in lightly doped GaAs/$Al_{0.3}Ga_{0.7}As$ superlattices. We study a weakly coupled superlattice, where we are able to observe the three lowest intersubband transitions having a linewidth of only 10 cm^{-1}. Then we concentrate on more strongly coupled superlattices, where we observe the absorption between two extended minibands. The line shape of the absorption does not show the symmetric double-peak structure, which is predicted by a simple model for the miniband dispersion. Possible reasons for this are discussed in terms of fluctuations and localization. At low enough temperature, the electrons freeze out into the donor ground state and the absorption is governed by impurity transitions. Remarkably, we are able to observe the pure $1s$-$2p_z$ donor transition.[14] Due to light polarization requirements, this transition has been seen so far only in a magnetic field perpendicular to the growth axis, when all p states are mixed and the selection rules relaxed.[15] A variational calculation of the impurity energy levels gives excellent agreement with the observed transition frequencies and shows that the $2p_z$ state is pinned below the $n=2$ miniband.

The paper is organized as follows. In Sec. II we provide some theoretical background for the interminiband absorption, and present the variational calculation for the impurity levels for a variety of superlattice parameters. Section III describes the experimental procedure and the sample parameters. In Sec. IV we present the results and compare them with the calculations. The paper is summarized in Sec. V.

II. THEORY

A. Interminiband absorption

The superlattice energy levels and band structure are readily calculated in the envelope function approach.[16] We want to focus, however, on the qualitative features of transitions between minibands. The absorption coefficient is proportional to the transition rate,[17] which is given by

$$W(\hbar\omega)=\frac{2\pi}{\hbar}\sum_{n<m}\sum_{k_z}|\langle\psi_m(z,k_z)|eEz|\psi_n(z,k_z)\rangle|^2 \times[f_n(k_z)-f_m(k_z)] \times\delta(E_m(k_z)-E_n(k_z)-\hbar\omega)\ . \quad (1)$$

In the above expression we consider only light polarized along the superlattice axis. If we assume the in-plane dispersion to be parabolic, then the integration over

the in-plane wave vector [already performed in Eq. (1)] does not give any contribution to the transition rate. e is the electronic charge, E the electric-field amplitude of the light. $\psi_n(z,k_z)$ and k_z denote the envelope function and the wave vector along the superlattice axis (z direction), respectively, and $f_n(k_z)$ are the electron occupancies of the different bands. In order to derive a simple analytic expression for $W(\hbar\omega)$ we consider the idealized case $n=1$, $m=2$, and $f_1=1$, $f_2=0$, i.e., we restrict ourselves to a filled bottom miniband and one empty excited miniband. This is a good approximation as long as the separation of the two lowest minibands is greater than $k_B T$, and the width of the bottom miniband is smaller than $k_B T$. Then we have

$$W(\hbar\omega)=\frac{2\pi}{\hbar}\sum_{k_z}|\langle\psi_2|eEz|\psi_1\rangle|^2\delta(E_2(k_z)-E_1(k_z)-\hbar\omega)\ . \tag{2}$$

We now use the tight-binding expression for the miniband dispersion

$$\begin{aligned}E_1(k_z)&=E_1+\Delta_1[1-\cos(k_z d)]\ ,\\ E_2(k_z)&=E_2+\Delta_2[1+\cos(k_z d)]\ .\end{aligned} \tag{3}$$

Here, d is the superlattice period, E_1 and E_2 are the bottom band edges of the two lowest minibands, and $2\Delta_1$ and $2\Delta_2$ are their respective widths. If we take the matrix element outside the integral (we numerically checked the very weak k_z dependence), we can perform the k_z integration, which gives

$$W(\hbar\omega)=\frac{e^2E^2}{m^*\omega}f_{12}[(\Delta_1+\Delta_2)^2-(\hbar\omega-E_2+E_1-\Delta_2+\Delta_1)^2]^{-1/2}\ . \tag{4}$$

In (4) we have expressed the z matrix element by the oscillator strength f_{12}, which is 0.96 for an infinite quantum well, and very close to this value also for superlattices, if the barriers are reasonably high. m^* is the effective mass. Equation (4) has two singularities, for the photon energies $\hbar\omega=E_2-E_1-2\Delta_1$ and $\hbar\omega=E_2-E_1+2\Delta_2$. Figure 1(a) shows their physical origin. The two singularities correspond to the transitions at the center and the edge of the Brillouin mini zone, at $k_z=0$ and $k_z=\pi/d$. (Recently, the states at the edge of the Brillouin minizone[18] have been observed in photoluminescence excitation spectroscopy.[19,20]) There the dispersions of the two minibands are parallel, resulting in critical points in the joint density of states. In Fig. 1(b), the joint density-of-states function is plotted for illustration (solid curve). It is clear that in reality the singularities will be smeared out and broadened by scattering processes and layer thickness fluctuations, which might seriously impede their observability. To illustrate the theoretical influence of scattering, we have replaced the δ function in Eq. (2) by a Lorentzian with a half-width at half-maximum of Γ, and performed the integration numerically. The result is shown as a dashed curve in Fig. 1(b) for $\Gamma=0.4(\Delta_1+\Delta_2)$.

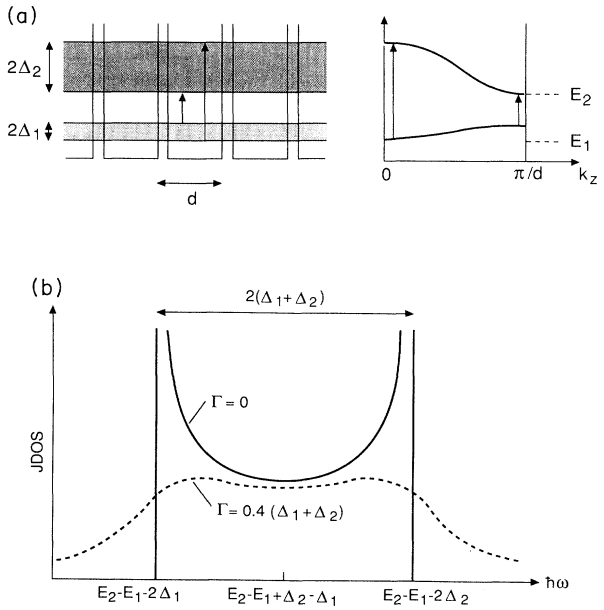

FIG. 1. (a) Schematic of the interminiband absorption in real space (left) and k space (right). (b) Joint density of states vs photon energy for no broadening (solid curve), and Lorentzian broadening (dashed curve).

B. Confined donor states: variational calculation

Most of the theoretical calculations of the binding energy of donor states address the single-quantum-well problem.[21–23] This is a very good approximation for the case of a weakly coupled superlattice (i.e., wide barriers). Here we are interested in the opposite limit of a strongly coupled superlattice. We will present a variational calculation of the energy of the four-lowest donor states in the absence of a magnetic field. We also calculate the $2s$ state which can be observed through a two-photon experiment.

Chaudhuri[24] has investigated the influence of the neighboring quantum wells on the binding energy of the $1s$ state of a donor in the center of the quantum well of a superlattice. Because only the adjacent wells were included in the calculation (barriers of semi-infinite thickness were introduced beyond the adjacent wells) the model of Ref. 24 does not work for superlattices with very thin barriers. This calculation will be generalized here: (i) to include all quantum wells of a superlattice, and (ii) the excited states of the donor states will also be calculated. Lane and Greene[25] calculated the effect of finite-width barriers upon the binding energy of the shallow donor states $1s$ and $2p_{x,y}$ in a GaAs/$Al_xGa_{1-x}As$ superlattice. Numerical results were presented for a superlattice with quantum well width $w=a_0\approx 100$ Å and barrier widths $b=a_0$, $2a_0$, ∞ ($a_0=\hbar^2\epsilon/m^*e^2$ is the effective Bohr radius). In the present paper we also calculate the $2s$ and $2p_z$ states, and present results for $b\ll a_0$.

Consider an isolated donor at position $(0,0,z_0)$ in a superlattice with well width w, barrier width b, and barrier height V_0. The electron mass in the quantum wells is m_w

and in the barriers m_b. This problem is described by the Hamiltonian

$$H=H_z-\frac{\hbar^2}{2m^*(z)}\left[\frac{\partial^2}{\partial x^2}+\frac{\partial^2}{\partial y^2}\right]-\frac{e^2}{\epsilon(z)[x^2+y^2+(z-z_0)^2]^{1/2}}\ , \tag{5}$$

where

$$H_z=-\frac{\hbar^2}{2}\frac{\partial}{\partial z}\frac{1}{m^*(z)}\frac{\partial}{\partial z}+V(z) \tag{6}$$

is the Hamiltonian for electron motion along the growth direction of the superlattice and $V(z)$ is the superlattice potential.

A variational calculation will be made for the energy levels of this hydrogenic-type problem. The variational wave function is taken to be the product of two functions

$$\Psi(x,y,z)=F_n(z)\phi_\mu(x,y,z-z_0)\ , \tag{7}$$

where $F_n(z)$ is a solution of the Schrödinger equation $H_zF_n(z)=E_nF_n(z)$ with zero average momentum. It is the wave function corresponding to the bottom of miniband n. The second part $\phi_\mu(x,y,z,-z_0)$ describes the localized donor state μ for a donor at $(0,0,z_0)$.

A standard calculation gives

$$F_n(z)=\begin{cases}Ae^{i\alpha z}+Be^{-i\alpha z}, & 0<z<w\\ Ce^{\beta z}+De^{-\beta z}, & -b<z<0\\ e^{ikdl}F(z-ld), & ld-b<z<w+ld\ ,\end{cases} \tag{8}$$

with $d=w+b$ the period of the superlattice, k the electron wave vector in the z direction, and l an integer. The coefficients of the wave function are given by

$$A=e^{-\alpha a}e^{-kd}-\cosh\beta b+i\frac{\beta}{\alpha}\frac{m_w}{m_b}\sinh\beta b\ ,$$

$$B=A^*\ ,$$

$$C=\frac{1}{2}\left[1+i\frac{\alpha}{\beta}\frac{m_b}{m_w}\right]A+\frac{1}{2}\left[1-i\frac{\alpha}{\beta}\frac{m_b}{m_w}\right]B\ ,$$

$$D=C^*\ ,$$

and we introduced $\alpha=\sqrt{2m_wE_n}/\hbar$ and $\beta=\sqrt{2m_b(V_0-E_n)}/\hbar$. The energy momentum relation is determined by the transcendental equation

$$\cos(kd)=\cos(\alpha a)\cosh(\beta b)-\frac{1}{2}\left[\frac{\alpha}{\beta}\frac{m_b}{m_w}-\frac{\beta}{\alpha}\frac{m_w}{m_b}\right]\sin(\alpha a)\sinh(\beta b)\ . \tag{9}$$

In Eq. (7) only the states with $k=0$ are needed. The second part in Eq. (7) describes the binding of the electron to the impurity due to the Coulomb interaction and will be taken similar in form to the standard hydrogen wave functions, but with the inclusion of parameters to allow for the difference in the isotropic hydrogen problem. The energy and length scales for the Coulomb part of the problem are the effective Rydberg $R=e^2/2\epsilon a_0^2$ and the effective Bohr radius a_0, respectively. For GaAs we have $\epsilon=12.5$ and $m^*/m_e=0.067$ which results in $R=5.834$ meV and $a_0=98.73$ Å. The wave functions expressed in these units are chosen as

$$\begin{aligned}\Psi_{1s}(x,y,z)&=F_1(z)e^{-\bar{r}\kappa}\ ,\\ \Psi_{2s}(x,y,z)&=F_1(z)e^{-\bar{r}\kappa}(1-\bar{r}\kappa)\ ,\\ \Psi_{2p_\pm}(x,y,z)&=F_1(z)e^{-\bar{r}\kappa}(x\pm iy)\ ,\\ \Psi_{2p_z}(x,y,z)&=F_2(z)e^{-\bar{r}\kappa}\ ,\end{aligned} \tag{10}$$

where we introduced $\bar{r}=(x^2+y^2+\nu z^2)^{1/2}$, and κ and ν are variational parameters. The above four states are orthogonal to each other and have the same symmetry as the corresponding three-dimensional (3D) hydrogen states. The energy is determined by minimizing

$$E_i=\frac{\langle\Psi_i|H|\Psi_i\rangle}{\langle\Psi_i|\Psi_i\rangle} \tag{11}$$

with respect to the two variational parameters κ and ν. Note that the above choice of wave functions leads to the correct 3D and 2D limits. The 3D limit is obtained by letting $w\to\infty$, which results in $F_1(z)\to1$, $F_2(z)\to z$ and the variational calculation gives for the $1s$ state the parameters $\kappa=\nu=1$ and for the energy $E_{1s}=-R$. The $2s,2p_{x,y},2p_z$ states have $\kappa=0.5$, $\nu=1$, and $E_{2s}=E_{2p_{x,y}}=E_{2p_z}=-R/4$. If one takes $w\to0$ for finite V_0 a different 3D limit is obtained but now for an impurity in the barrier material where the electron has a different mass m_b and the energy is shifted by V_0. The 2D limit is obtained for $w\to0$ and $V_0\to\infty$ (with $b\neq0$) and gives the standard results, e.g., for the $1s$ state it leads to $\kappa=2$ and $E_{1s}-E_1=-4R$.

The explicit analytical result for Eq. (11), in terms of the two variational parameters, is quite lengthy but straightforward to obtain and, therefore, will not be given. The numerical results for the energy versus the well width of a donor in the center of a quantum well of the superlattice is depicted in Figs. 2(a) and 2(b) for a barrier with width $b=50$ and 11 Å, respectively. The energy of the $1s$, $2s$, $2p_{x,y}$, and $2p_z$ states are shown together with the lowest minibands (shaded area). Note that the presence of the barriers lift the degeneracy of the $n=2$ donor state into three distinct states: $2s,2p_{x,y}$, and $2p_z$. The $2p_{x,y}$ state is still twofold degenerate, i.e., $E_{2p_{x,y}}=E_{2p_\pm}$. A magnetic field along the z axis will lift this degeneracy and results into $E_{2p_+}>E_{2p_-}$. Our numerical calculation involves the numerical calculation of a 2D integral and consequently a numerical 2D variational calculation of each of the four donor states. The following parameters were taken: $\epsilon=12.5$ (although our numerical program allows for different static dielectric constants in the wells and the barriers we have taken the same value of ϵ in the wells and the barriers), $V_0=227.9$ meV, $m_w/m_0=0.067$, and $m_b/m_0=0.0919$. The results for $b=50$ Å are practically the same as for the single-quantum-well case (i.e., $b\to\infty$, not shown in the figure) when $w>300$ Å. In this case the width of the minibands

is very small. The $b=11$ Å case corresponds to a strong interacting superlattice, which is characterized by wide minibands. Note that for $w\rightarrow\infty$ the 3D results are obtained for the hydrogenic states. Also note that the $1s, 2s, 2p_{x,y}$ states are always below the bottom of the first miniband. It is interesting to observe that the $2s$ and the $2p_{x,y}$ states are very close in energy and they cross around 400 Å, i.e., for $w<400$ Å the $2s$ state has a lower energy than the $2p_{x,y}$ state. That $E_{2s}\approx E_{2p_{x,y}}$ is not surprising because (i) in 3D $E_{2s}=E_{2p_{x,y}}$, and (ii) the superlattice only modifies the electron wave function in the z direction where the $2s$ and the $2p_{x,y}$ states have the same symmetry; they are an even function under $z\rightarrow -z$. This is different for the $2p_z$ state which is an odd function under $z\rightarrow -z$ which is the symmetry exhibited by the second miniband. This explains why the $2p_z$ state is always below the bottom of the second miniband. However, for wide well width it is even lower than the first miniband. It crosses the first miniband around $w\approx 600-700$ Å for the barrier widths of Fig. 2.

The wave functions squared for the $2p_z$ state are shown in Figs. 3(a) and 3(b) for $w=200$ Å and $b=50$, 11 Å as a function of $(\rho=(x^2+y^2)^{1/2},z)$. The impurity is at the origin, i.e., $(\rho,z)=(0,0)$, and the position of the barriers is indicated by the solid areas. These figures illustrate (i) the spreading of the wave function over several quantum wells, and (ii) in case of wide barriers the donor wave

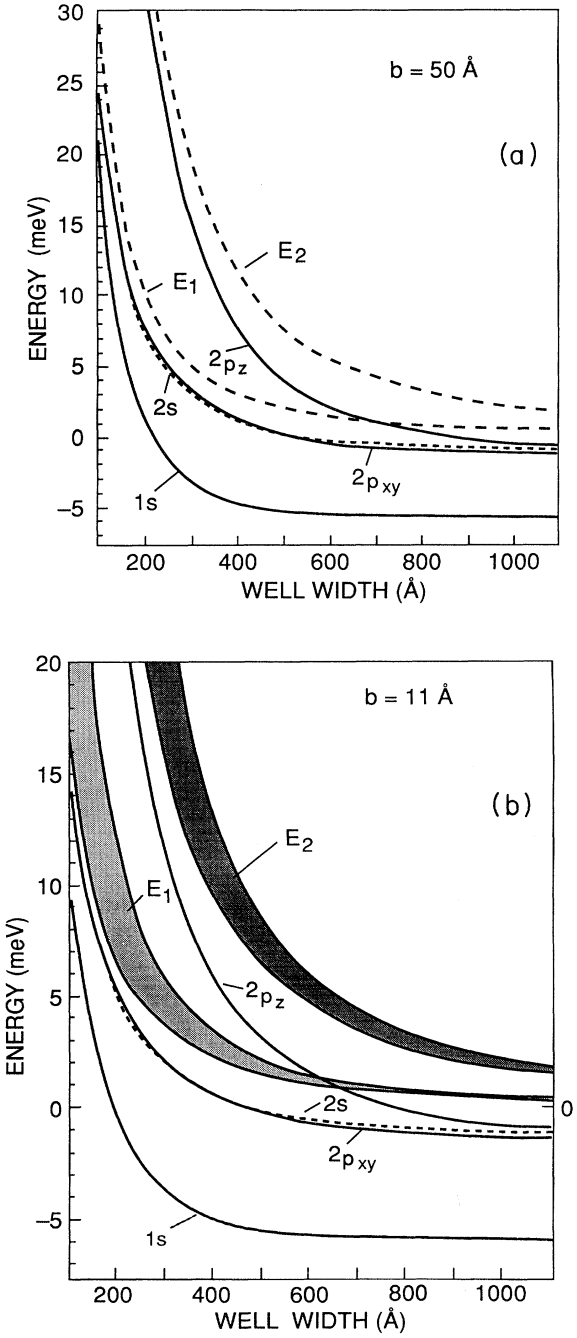

FIG. 2. The donor energy levels of an impurity in the center of the quantum well and the lowest minibands of a superlattice as a function of well width with barrier width (a) $b=50$ Å, and (b) $b=11$ Å.

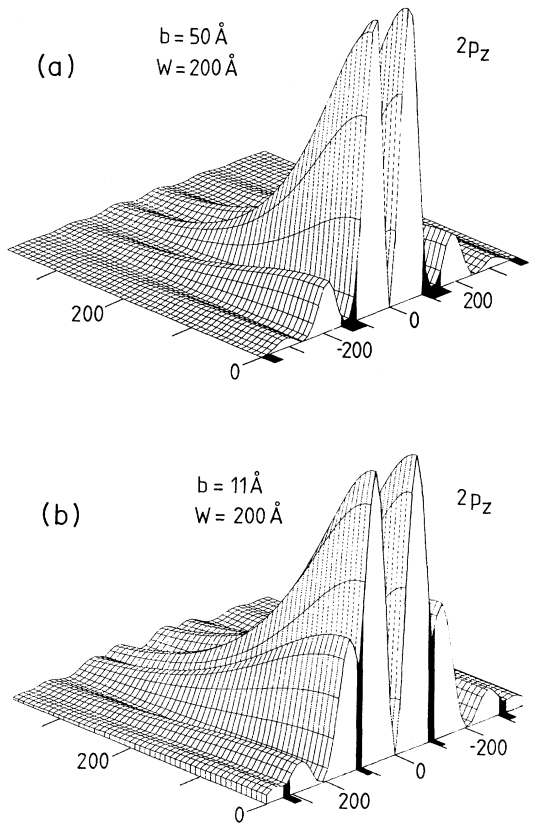

FIG. 3. The probability distribution of the $2p_z$ donor state in the $(\rho=(x^2+y^2)^{1/2},z)$ plane for an impurity located at the origin which is the middle of a quantum well. The superlattice has quantum wells of width $w=200$ Å and barriers of (a) $b=50$ Å, and (b) $b=11$ Å. The position of the barriers is indicated by the solid areas.

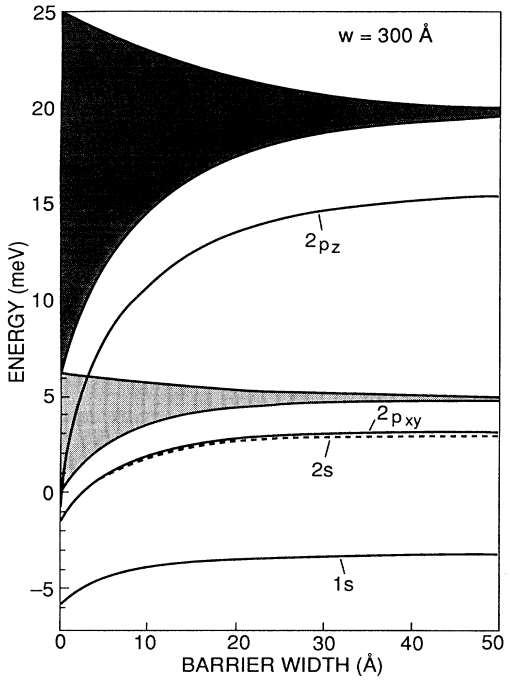

FIG. 4. The same as in Fig. 2 but now as function of the barrier width and for fixed width of the quantum wells $w = 300$ Å.

function is more squeezed towards the impurity ion than for narrow barriers.

In Fig. 4 the energy levels and minibands are shown as function of the barrier width for a superlattice with a fixed quantum-well width of $w = 300$ Å. In the limit of $b \to 0$ the known 3D results are obtained $E_{1s} = -5.83$ meV and $E_{2s} = E_{2p_{x,y}} = E_{2p_z} = -1.46$ meV. In the limit of very large barrier width the single-quantum-well result is obtained with $E_{1s} = -3.81$ meV, $E_{2s} = 2.71$ meV, $E_{2p_{x,y}} = 2.79$ meV, $E_{2p} = 14.41$ meV, and the quantum-well energy levels $E_1 = 4.94$ meV and $E_2 = 19.75$ meV. This results in the binding energies $E_{1s} - E_1 = -8.75$ meV and $E_{2p_{x,y}} - E_1 = -2.15$ meV, which were already obtained by Greene and Bajaj in Ref. 14, and $E_{2s} - E_1 = -2.23$ meV and $E_{2p_z} - E_2 = -5.34$ meV. With decreasing barrier thickness the donor wave function spread more to the adjacent wells which reduces the binding energies. For example, for $w = 300$ Å and $b = 25$ Å (11 Å) we found $E_{1s} - E_1 = -7.85$ (-7.43) meV, $E_{2p_{x,y}} - E_1 = -1.55$ (-1.53) meV, $E_{2s} - E_1 = -1.78$ (-1.70) meV, and $E_{2p_z} - E_2 = -3.89$ (-3.91) meV. The existing calculations with the single-well approximation become less adequate with decreasing barrier thickness.

III. EXPERIMENTAL DETAILS

The samples investigated were GaAs/$Al_{0.3}Ga_{0.7}As$ superlattices grown either by organometallic chemical vapor deposition (OMCVD) or molecular-beam epitaxy (MBE) on a semi-insulating GaAs substrate. The sample parameters (nominal thicknesses) are given in Table I. In the OMCVD samples the light n-type doping was unintentional, achieved by adjusting the growth temperature. The MBE sample was doped intentionally. All superlattices had a total thickness of about 6 μm. The electron mobilities at 77K were between 20 000 and 50 000 $cm^2/V\,s$, depending on the impurity concentration. Ohmic contacts were formed by depositing and alloying Ni-Au-Ge. Grating couplers (periods of 8 and 12 μm) were made by evaporating TiAu on a photolithographically defined pattern (area of 3×4 mm^2), and subsequent lift-off.

The absorption measurements were performed in a slow-scan Fourier transform spectrometer. The sample temperature could be varied between 1.5 and 200 K. Since the low-doped samples exhibit rather weak absorption, we employed a highly sensitive modulation technique. A modulation voltage is applied between the grating, which acts as a Schottky gate, and the Ohmic contacts.[12] Thus the superlattice is periodically switched between two different states: with a high enough (≈ 10 V) negative voltage on the gate, the superlattice is totally depleted (no electrons), whereas with a small positive voltage (≈ 0.5 V), the bands are flat (electrons present). As a consequence, the signal is proportional to the transmission without electrons minus the transmission with electrons, and thus small transmission changes can be measured with high sensitivity. The electric field does not influence the measurement, because regions with electric field are depleted, i.e., contain no electrons. With this method it is possible to take absorption spectra in a wavelength range $\lambda/n_r > D$, where n_r is the refractive index and D is the grating period.[10]

IV. RESULTS AND DISCUSSION

First we discuss the results on the (400 Å)/(50 Å) superlattice (we will use this notation from now on). Due to the rather thick barriers of 50 Å the four-lowest minibands have a width smaller than 1 meV. Since this is nar-

TABLE I. Characteristics of the different samples, with w the well width, b the barrier width, and n_e the electron density.

Sample	w (Å)	b (Å)	n_e (cm^{-3})	Growth method
No. 1	400	50	1.5×10^{15}	OMCVD
No. 2	320	11	8×10^{15}	OMCVD
No. 3	260	11	5×10^{15}	OMCVD
No. 4	230	11	2.5×10^{15}	MBE

rower than typical broadening by scattering, the states can be regarded as localized quantum-well states without energy dispersion. On the other hand, a barrier thickness of 50 Å is thin enough that all periods of the superlattice are electrically shorted in the vertical direction, which is important in connection with the measurement technique. Figure 5 shows absorption spectra between 20 and 200 cm^{-1} (2.5–25 meV photon energy) for different temperatures between 6 and 130 K. The grating had a period of 12 μm. Even though the spectra are quite complex, it is relatively easy to assign the various transitions, especially if their temperature dependence is studied. At low temperatures the spectrum will be dominated by donor transitions. At high temperatures, when all donors are ionized, we will observe intersubband transitions. The relatively wide well thickness of 400 Å is interesting in the sense that it allows thermal population of the $n=2$ and 3 subbands at not too high temperatures. As a consequence, we are able to observe the three lowest intersubband transitions at 130 K. The 2–3 transition is even stronger than the 1–2 transition, because it has approximately twice the oscillator strength[3] [the absorption strength is proportional to the electron occupancy times the oscillator strength, see Eq. (1), Ref. 26].

We want to point out the very narrow linewidth (10 cm^{-1} or 1.25 meV) as compared to previously reported intersubband transitions. There are two main reasons for this: since most of the previous work concentrated on narrow wells, the two most important broadening mechanisms were well width fluctuations and optical phonon scattering. Both mechanisms become virtually negligible in the present superlattice: Fluctuations of one monolayer correspond to a broadening of only 0.1 meV (1 cm^{-1}), and the first three subbands lie below the optical phonon energy, thus making optical phonon emission impossible. The linewidth is then mostly limited by ionized impurity scattering. The observation of three intersubband absorption lines allows an accurate determination of the actual well width, by comparison with the envelope function calculation. Figure 6 shows the theoretical transition energies as a function of well width. Excellent agreement is obtained assuming a well width of 420 Å, as compared to the nominal width of 400 Å.

Towards lower temperature the higher intersubband transitions vanish, and donor transitions appear. It is well known that donor transitions in quantum wells and superlattices are generally much broader than in bulk material, because the binding energies depend on the position of the donor along the growth axis.[21,27] If the material is homogeneously doped as in the present case, absorption spectra in principle probe a continuum of different transition energies. (In contrast, Jarosik *et al.*[28] used samples that were exclusively doped in the well centers.) Since the binding energy versus donor position has extrema at the well and barrier center, there are two maxima in the density of states associated with them. Bastard[21] showed that for well widths larger than the effective Bohr radius, which is about 100 Å, the peak corresponding to the well center becomes dominant, which should be the case in the present sample. Certainly the line shape of the donor transitions still will be influenced by impurities located elsewhere. For a realistic description, the binding energies would have to be calculated as a function of donor position along the growth axis, and

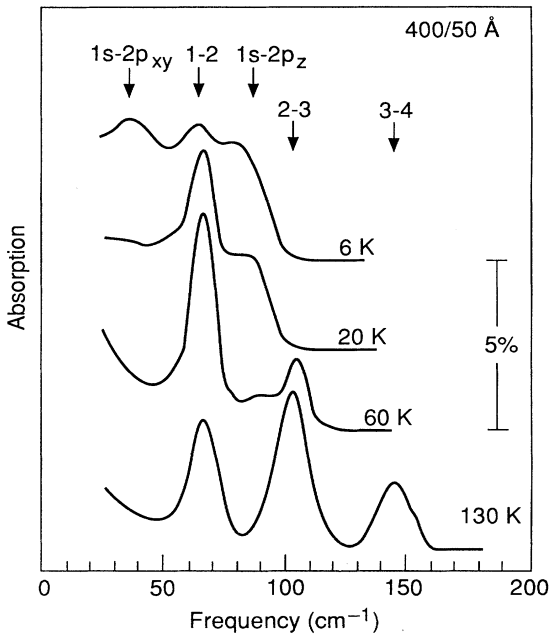

FIG. 5. Absorption spectrum from the (400 Å)/(50 Å) superlattice at different temperatures as indicated. The curves are shifted vertically, with the zero defined on the high-frequency side.

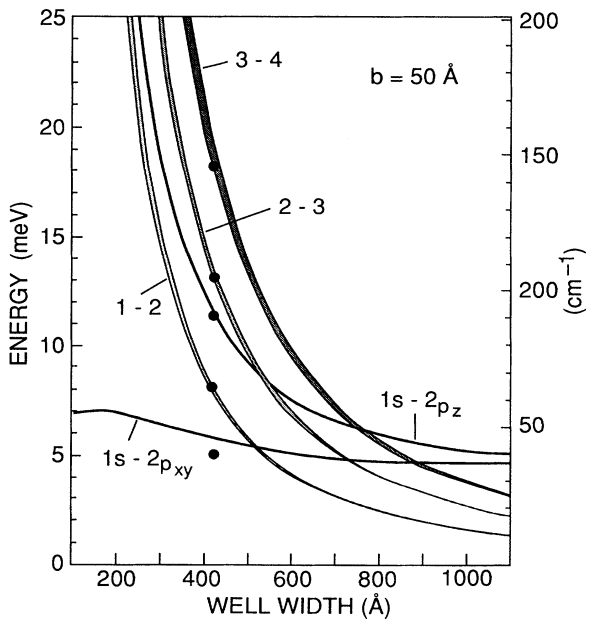

FIG. 6. Intersubband and donor transitions for a barrier width of 50 Å as a function of well width. The symbols are the experimental results from the (400 Å)/(50 Å) superlattice.

subsequently averaged. This is, however, beyond the scope of the present paper. We will compare the experimental results with the calculation for donors in the well center.

There are two low-temperature peaks in Fig. 5, at 40 and about 90 cm^{-1}. The agreement with the theoretical transition energies in Fig. 6 is better than expected, especially for the $2p_z$ state. The $1s$-$2p_{x,y}$ transition lies somewhat low, probably due to some influence of well-edge or barrier dopants. We point out that all transitions in Fig. 5, except the $1s$-$2p_{x,y}$ are facilitated by the grating, since they all require the polarization to be perpendicular to the layers. Previously, the $1s$-$2p_z$ transition has only been observed in a magnetic field parallel to the layers[15] (except for a Raman scattering experiment by Perry *et al.*[29]). In that case the $2p_z$ state has admixtures from the $2p_x$ and $2p_y$ states, and the polarization selection rules are relaxed.

We turn now to the discussion of the other samples, which are all strong coupling superlattices with finite miniband width and dispersion along the growth direction. The number of investigations devoted to far-infrared spectroscopy of strong coupling superlattices so far is rather limited, dealing mostly with tunneling cyclotron resonance[30] and very recently with intraminiband absorption.[12]

We chose to achieve strong interwell coupling by using very thin barriers (11 Å or 4 monolayers), instead of a short period. This choice keeps the relevant frequencies below the reststrahlen region, and the electrons unaffected by optical phonon emission. In Table II the calculated energies of the first and second miniband are given for our three strong coupling superlattices together with the expected range of interminiband absorption. For all samples we recorded a cyclotron resonance absorption spectrum to check the broadening induced by scattering processes. The cyclotron resonance linewidth was 10–13 cm^{-1} for the (230 Å)/(11 Å) and the (260 Å)/(11 Å) superlattice, and 20 cm^{-1} for the (320 Å)/(11 Å) superlattice, both considerably smaller than the expected miniband absorption width. Consequently, the miniband dispersion should be well established.

Figures 7 and 8 show the absorption spectra for the (260 Å)/(11 Å) and (230 Å)/(11 Å) superlattices at different temperatures as indicated (grating period of 8 μm). The spectra in Fig. 7 consist of a low frequency tail, which is due to the $1s$-$2p_{x,y}$ donor transition at low temperature, and free-carrier absorption at high temperatures, and two peaks at 105 and 150 cm^{-1}, which become equally strong at about 30 K. It is tempting to ascribe these two peaks to the singularities in the joint density of states of the interminiband transition. Closer inspection,

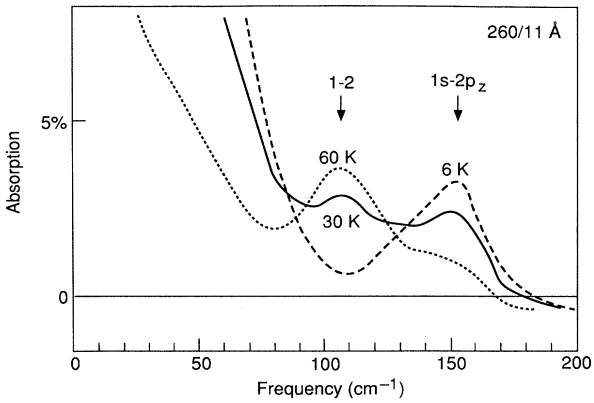

FIG. 7. Absorption spectrum for the (260 Å)/(11 Å) superlattice at different temperatures.

however, shows that this explanation is not consistent with the temperature dependence. The interminiband absorption could be expected to exhibit one high-energy peak at low temperature (but high enough to ionize enough donors), but two peaks at high temperature, as soon as the top of the lower miniband becomes thermally populated. Both peaks should remain equally strong up to high temperatures. This is evidently not the case in the experiment, where the low-energy peak grows at the cost of the high-energy peak and only one peak remains also at high temperatures. Consequently we have to attribute the high-energy peak again to the $1s$-$2p_z$ donor transition, and the low-energy peak represents the interminiband absorption. Still, a high-frequency tail persists even at high temperature, when all donors are ionized. The observed line shape does not agree with the model in Sec. II A, but is not a simple Lorentzian, either.

Figure 8 shows a low- and high-temperature spectrum for the (230 Å)/(11 Å) superlattice. At low temperature, a clear $1s$-$2p_z$ donor transition is observed. At high temperatures, when all the donors are ionized, the interminiband absorption is revealed. Here it is obvious that the spectral range of the interminiband transition and the donor transition overlap. The shape of the former is again unusual. The features are similar but more distinct than in the sample discussed before. The high-frequency tail could be argued to be a second bump, resulting from the second maximum in the joint density of states, but the relative sizes are not consistent with the simple model from Sec. II A. Even though we do not observe two well-resolved peaks, this is the first observation of a genuine interminiband transition, in the sense that the absorption width is much wider than for discrete energy

TABLE II. Calculated miniband energies and absorption ranges for the strong coupling superlattices.

Sample	E_1 (meV)	E_2 (meV)	Absorption range (meV)
(320 Å)/(11 Å)	3.4–5.1	14.0–20.3	8.9–16.9 (72–136 cm^{-1})
(260 Å)/(11 Å)	4.7–7.6	19.7–30.3	12.1–25.6 (98–206 cm^{-1})
(230 Å)/(11 Å)	5.7–9.5	23.9–38.2	14.4–32.5 (116–262 cm^{-1})

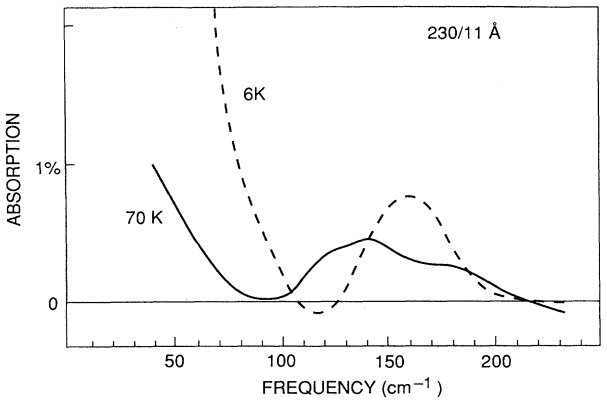

FIG. 8. Absorption spectrum for the (230 Å)/(11 Å) superlattice at different temperatures.

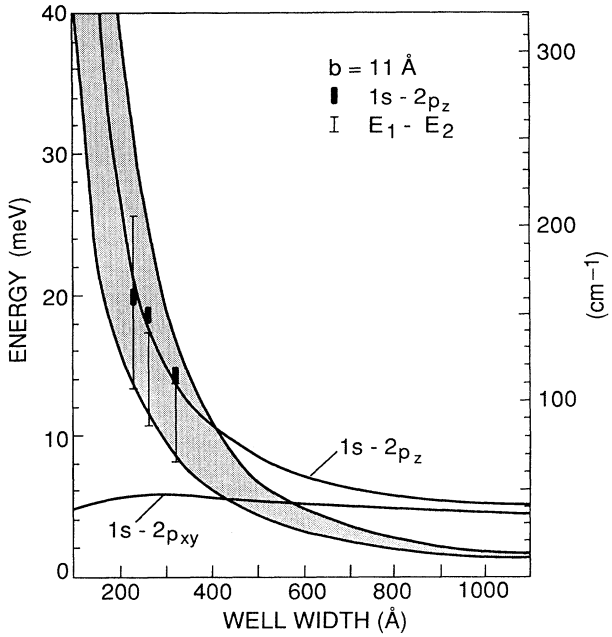

FIG. 9. Interminiband and donor transitions for a barrier width of 11 Å as a function of well width. The symbols represent experimental results from three samples.

levels. The absorption at very low frequencies is again governed by the $1s$-$2p_{x,y}$ transition and free-carrier absorption at low and high temperatures, respectively.

In Fig. 9 the theoretical transition energies for the $1s$-$2p_{x,y}$ $1s$-$2p_z$, and interminiband transition are plotted versus the well width for a barrier width of 11 Å. The experimentally observed values are represented by symbols. The exact width of the experimental interminiband absorption is somewhat ambiguous because of the unusual line shape. It is apparent, however, that it is narrower than the theoretical width. The onset of the absorption at low frequencies generally agrees with the prediction, but it does not extend up to high enough frequencies. For the $1s$-$2p_z$ donor transition we assume a line shape with a peak at the resonance frequency, the solid rectangles in Fig. 9 then represent just the line center. The agreement for the impurity transitions is excellent. This indicates that we are observing mainly impurities located in the center of the wells.

Before we conclude, we want to speculate on the reason for the observed width and shape of the interminiband absorption. It is well known that all layered semiconductor structures suffer from unavoidable layer thickness fluctuations. Even though well width fluctuations are not very significant in the present superlattices due to the relative wide wells, barrier width fluctuations have strong influence on the minibands. For example, in the (260 Å)/(11 Å) superlattice a barrier thickness of 3 monolayers would cause a width of 13 meV for the $n=2$ miniband, whereas 5 monolayers only correspond to 8.6 meV. If fluctuations are strong, they also lead to a partial localization of the electron states. Since the absorption line shape depends strongly on the dispersion in the superlattice direction, it can be distorted severely by localization. For example, the equal strength of the two absorption maxima relies on the symmetry of the dispersions in the vicinity of $k_z=0$ and $k_z=\pi/d$, which is apparently perturbed in the present samples. To better understand these effects, it seems desirable to measure the width of minibands with a variety of different methods (cf., for example, Refs. 12, 30, and 31), and to investigate theoretically the influence of fluctuations and localization[32] on the minibands.

V. SUMMARY

We have performed a detailed investigation of the far-infrared absorption spectrum of GaAs/$Al_{0.3}Ga_{0.7}As$ superlattices. The use of a grating coupler has enabled us to investigate intersubband and impurity transitions in a regime that is not easily accessible otherwise. We have shown that the three lowest intersubband transitions are observable at the same time at sufficiently high temperature, if the wells are wide enough. In strong-coupling superlattices, we have observed the transition between extended-state minibands. Here, some questions concerning the width and shape of the absorption are still open. Furthermore, we have studied the $1s$-$2p_z$ donor transition experimentally and theoretically, and obtained excellent agreement.

ACKNOWLEDGMENTS

We are grateful to S. J. Allen for insightful discussions and critically reading the manuscript. One of us (F.M.P.) was supported by the Belgian National Science Foundation.

*Present address: Institut für Halbleiterphysik, Universität Linz, A-4040 Linz, Austria, whereto all correspondence should be addressed.

†Permanent address: Department of Physics, University of Antwerp (UIA), B-2610 Wilrijk, Belgium.

[1]For reviews, see L. Esaki, IEEE J. Quantum Electron. **QE-22**, 1611 (1986); F. Capasso, K. M. Mohammed and A. Y. Cho, *ibid.* **QE-22**, 1853 (1986).

[2]For a review see, J. M. Mercy, Y.-H. Chang, A. A. Reeder, G. Brozak, and B. D. McCombe, Superlatt. Microstruct. **4**, 213 (1988).

[3]L. C. West and S. J. Eglash, Appl. Phys. Lett. **46**, 1156 (1985).

[4]B. F. Levine, C. G. Bethea, G. Hasnain, J. Walker, and R. J. Malik, Appl. Phys. Lett. **53**, 296 (1988).

[5]F. Stern, Phys. Rev. Lett. **33**, 960 (1974).

[6]B. F. Levine, R. J. Malik, J. Walker, K. K. Choi, C. G. Bethea, D. A. Kleinman, and J. M. Vandenberg, Appl. Phys. Lett. **50**, 273 (1987).

[7]L. Zheng, W. L. Schaich, and A. H. MacDonald, Phys. Rev. B **41**, 8493 (1990).

[8]D. Heitmann, J. P. Kotthaus, and E. G. Mohr, Solid State Commun. **44**, 715 (1982).

[9]D. Heitmann and U. Mackens, Phys. Rev. B **33**, 8269 (1986).

[10]M. Helm, E. Colas, P. England, F. DeRosa, and S. J. Allen, Jr., Appl. Phys. Lett. **53**, 1714 (1988).

[11]M. Helm, P. England, E. Colas, F. DeRosa, and S. J. Allen, Jr., Phys. Rev. Lett. **63**, 74 (1989).

[12]G. Brozak, M. Helm, F. DeRosa, C. H. Perry, M. Koza, R. Bhat, and S. J. Allen, Jr., Phys. Rev. Lett. **64**, 3163 (1990).

[13]W. J. Li, B. D. McCombe, F. A. Chambers, G. P. Devane, J. Ralston, and G. Wicks, Surf. Sci. **228**, 164 (1989).

[14]R. L. Greene and K. K. Bajaj, Phys. Rev.B **31**, 4006 (1985).

[15]G. Brozak, B. D. McCombe, and D. M. Larsen, Phys. Rev. B **40**, 1265 (1989).

[16]G. Bastard, Phys. Rev. B **24**, 5693 (1981).

[17]S. Nojima, Phys. Rev. B **41**, 10 214 (1990).

[18]H. Chu and Y.-C. Chang, Phys. Rev. B **36**, 2946 (1987).

[19]J. J. Song *et al.*, Phys. Rev. B **39**, 5562 (1989); B. Deveaud *et al.*, *ibid.* **40**, 5802 (1989).

[20]K. J. Moore, G. Duggan, A. Raukema, and K. Woodbridge, Phys. Rev. B **42**, 1326 (1990).

[21]G. Bastard, Phys. Rev. B **24**, 4714 (1981).

[22]C. Mailhiot, Y.-C. Chang, and T. C. McGill, Phys. Rev. B **26**, 49 (1982).

[23]R. L. Greene and K. K. Bajaj, Solid State Commun. **45**, 825 (1983).

[24]S. Chaudhuri, Phys. Rev. B **28**, 4480 (1983).

[25]P. Lane and R. L. Greene, Phys. Rev. B **33**, 5871 (1986).

[26]The experimental spectrum can also be used to estimate the relative grating-coupling efficiency over a certain frequency range; see Ref. 11.

[27]T. Duffeld, R. Bhat, M. Koza, M. C. Tamargo, J. P. Harbison, F. DeRosa, D. M. Hwang, P. Grabbe, and S. J. Allen, Jr., Solid State Commun. **60**, 557 (1986).

[28]N. C. Jarosik, B. D. McCombe, B. V. Shanabrook, J. Comas, J. Ralston, and G. Wicks, Phys. Rev. Lett. **54**, 1283 (1985).

[29]T. A. Perry, R. Merlin, B. V. Shanabrook, and J. Comas, Phys. Rev. Lett. **54**, 2623 (1985).

[30]T. Duffield, R. Bhat, M. Koza, F. DeRosa, K. M. Rush, and S. J. Allen, Jr., Phys. Rev. Lett. **59**, 2693 (1987); T. Duffield, R. Bhat, M. Koza, D. M. Hwang, F. DeRosa, P. Grabbe, and S. J. Allen, Jr., Solid State Commun. **65**, 1483 (1988).

[31]P. England, J. R. Hayes, J. P. Harbison, D. M. Hwang, and L.T. FLorez, Appl. Phys. Lett. **53**, 391 (1988); P. England, J. R. Hayes, E. Colas, and M. Helm, Phys. Rev. Lett. **63**, 1708 (1989).

[32]H. A. Fertig and S. Das Sarma, Phys. Rev. B **42**, 1448 (1990).